Congested shallow water model: floating object

Edwige Godlewski, Martin Parisot, Jacques Sainte-Marie, Fabien Wahl

CONGESTED SHALLOW WATER MODEL: FLOATING OBJECT

EDWIGE GODLEWSKI, MARTIN PARISOT, JACQUES SAINTE-MARIE,
AND FABIEN WAHL

Abstract. We are interested in the floating body problem on a large space scale. We focus on objects floating freely in the water such as icebergs or wave energy converters. The formulation of the fluid-solid interaction using the congested shallow water model for the fluid and Newton's second law of motion for the solid is given and a strong coupling between the two systems is explained. The energy transfer between the solid and the water is focused on since it is of major interest for energy production. A numerical resolution based on the coupling of a finite volume scheme for the fluid and a Newmark scheme for the solid is presented. An entropy correction based on an adapted choice of discretization for the coupling terms is made in order to ensure a dissipation law at the discrete level. Simulations are presented to validate the method and to show the feasibility of more complex cases.

1. Introduction

We are interested in the modeling of a floating body. In a previous work [12] we considered a congested shallow water model. A roof denoting an impermeable surface above the water flow which constrains the water surface was introduced in the cited work. In [12], the motion of the roof was prescribed, whereas in the present work, it is no longer the case, leading to the coupling of the equations modeling the fluid and the structure motion. Applications are floating icebergs, floating fragments during inondations or the production of sustainable energy using buoys.

Two main approaches are proposed in the literature to treat fluid-solid interaction.

The first dates back to Fritz John who proposed a mathematical formulation of the problem [16]. The fluid is described by a velocity potential with a linear model for the free surface evolution. The motion of the solid is supposed to be of small amplitude so that the interface between the water and the solid is constant in time. Finally the surface pressure is obtained using the linearized Bernoulli equation. Although the model is quite simplified, linear potential flow theory is still used in industrial context since it is not costly in CPU time, see [23]. However nonlinear terms play an important part for wave interaction. For instance the nonlinearity should be taken into account in simulations of wave energy converter farms. Improvements have been made to include nonlinear effects based on the boundary element methods [14] and an interface depending on time [17]. This progress needs higher CPU times and does not yet allow wave breaking.

Date: September 11, 2018.

2010 *Mathematics Subject Classification.* 35Q35, 35L65, 76B07, 74F10, 76M12.

Key words and phrases. shallow water equations, wave-body interaction, congested hyperbolic model, coupling, entropic scheme.

The second are Navier-Stokes CFD computations. This approach is considerably used in blood flow [28, 9], where the characteristics of aortic flow are studied.

Some works use Navier-Stokes CFD computations for the simulation of the flow around a yacht [26] or wave energy converters [1, 24, 30]. This approach couples the fluid usually expressed in a Eulerian frame and the solid usually expressed in a Lagrangian frame. The difficulty comes from the mesh. A moving grid with front tracking methods or a fixed mesh with fictitious fluid domain can be considered. The first one perfectly catches the interface but needs a moving mesh while the second is less accurate on the position of the interface but the mesh is fixed. However this strategy implies high CPU times and does not make these methods suitable for engineering optimization.

To take advantage of the benefits from each approach, a coupling has been proposed [29]. Since the viscosity is not considered in potential flow theory, it can hardly been included in the coupling.

Recently the nonlinear floating body problem was reformulated in the framework of vertical-integrated models [20]. A vertical movement of the body is considered so that the interface between the congested and the free surface domain is fixed in time and continuity of the unknowns is assumed at the interface. The surface pressure is then obtained by an elliptic equation.
An analysis of this shallow water type model in the two dimensional case with radial symmetry is done in [5]. In a more general framework the well-posedness of the model in the one dimensional case has been proven in [15], relaxing the assumption of vertical lateral walls. The description of the interface position is dealt with.
A numerical resolution in one dimension of the model proposed in [20] is done in [6]. Each domain can be solved by the most appropriate numerical strategy but transmission conditions have to be written at the interface. Since discontinuous solutions can appear in hyperbolic models, the latter conditions can be tricky to handle.

In [12] we have proposed a uniform numerical resolution which eliminates the description of the interface and the transition conditions between the congested and the free surface domain. The surface pressure is seen as a Lagrange multiplier associated to a constraint.

These models based on depth-averaging cannot modelize wave breaking but nonlinear terms are accounted for. Simpler than the Navier-Stokes equations but still physically relevant, their resolution is less CPU consuming since the computational domain does not depend on time. For optimization processes this seems interesting, especially when large domains are considered.

In the present work, we give a formulation of the floating body problem taking into account a freely floating object, i.e. translating and rotating. A choice of discretization for the different operators is proposed in order to assure a strong coupling between the two systems. We use a Newmark scheme for the solid and adapt the numerical strategy given in [12] for a 'fixed roof' to the coupling. Furthermore our method allows to write the energy of the coupled fluid-solid system. The energy transfer between the fluid and the solid is indeed a challenging problem and of major interest in energy production using buoys. From a mathematical point of view, the energy balance, acting as an entropy, is an argument for the existence of

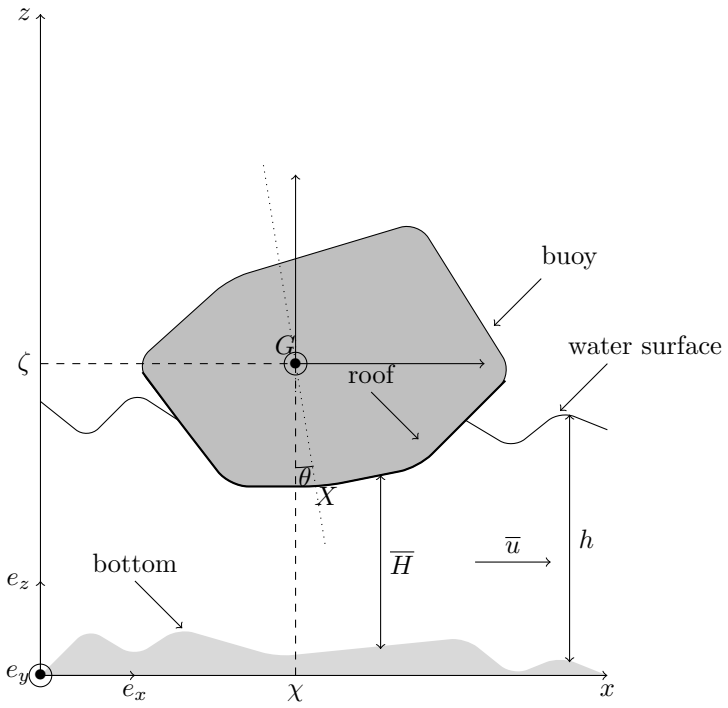

FIGURE 1. Buoy configuration

long time solutions.

In Section 2 the formulation at the continuous level is given. In Section 3 we explain the numerical strategy. A first naive non-entropy satisfying approach is considered followed by an entropy correction. Finally we show simulations in a one dimensional framework to validate our approach.

2. Mathematical modeling

Let us start by recalling the shallow water model for constrained flow.

2.1. **Fluid dynamics.**

In [12] a shallow water type model with an additional congestion constraint modeling a 'roof' is proposed. Let us briefly introduce this model which is derived from the Navier-Stokes equations.
A flow contained between two surfaces respectively called roof and bottom is considered. The two surfaces can be parametrized by two given mono-valued smooth enough functions $R(x,t)$ and $B(x,t)$ (see Figure 1) which satisfy $B(x,t) \leq R(x,t)$. The opening $\overline{H}$ between the roof and the bottom is defined by

$$\overline{H}(x,t) = R(x,t) - B(x,t).$$

We consider a one dimensional given domain $\Omega_x \subset \mathbb{R}$. In practice the domain Ω_x will be bounded but for simplicity the boundary conditions will not be detailled.

The unknowns of the model are the water depth h, the vertical-averaged horizontal velocity $\overline{u}$ and the surface pressure p_η which satisfy

$$\begin{cases} \partial_t h & + \partial_x \left(h\overline{u}\right) & = 0 \\ \partial_t \left(h\overline{u}\right) & + \partial_x \left(h\overline{u}^2 + \dfrac{g}{2}h^2\right) & = -h\partial_x \left(gB + p_\eta\right) \end{cases} \tag{1}$$

with g the gravitational constant.
In addition, the constraint

$$\min\left(\overline{H} - h, p_\eta - P\right) = 0 \tag{2}$$

has to be satisfied where $P(x,t)$ denotes the given atmospheric pressure.
In the following, the atmospheric pressure is taken constant in time and space and for simplicity equal to zero, i.e. $P = 0$.
Finally the system (1)-(2) is completed with the initial conditions $h(x,0) = h^0(x)$ and $\overline{u}(x,0) = \overline{u}^0(x)$.
An energy balance law can be written.

Lemma 2.1. *There exists a flux $\mathcal{G}$ such that any smooth enough solution of the congested shallow water model (1)-(2) satisfies the following energy balance law*

$$\partial_t \mathcal{E} + \partial_x \mathcal{G} = -p_\eta \partial_t R + \left(gh + p_\eta\right)\partial_t B$$

with the mechanical energy

$$\mathcal{E} = \frac{1}{2}h\overline{u}^2 + gh\left(B + \frac{h}{2}\right)$$

and the energy flux $\mathcal{G}$ defined in [12].

Proof. The proof is done in [12, Proposition 1.3]. □

In the present work, if $B(x,t)$ is still a given function, this is no longer the case for $R(x,t)$. The interaction between the fluid and the roof is considered, i.e. $R(x,t)$ is now an unknown of the problem and its evolution has to be determined.

Note that the modeling of submerged objects is not allowed by the choice of modeling for the fluid since the model considers only one water height. Thus in the following, we will restrict ourselves to objects that cannot be submerged. More precisely, we suppose that a line segment between a point on the fluid surface and its projection on the horizontal domain Ω_x does not cross the object.

2.2. **Solid dynamics.** Let us describe the planar motion of a floating object. The reader can refer to [18] for more details about solid dynamics. The scalar product between two vectors v_1 and v_2 is denoted $v_1 \cdot v_2$ and the cross product $v_1 \times v_2$.
We consider a homogeneous solid body $\mathcal{B}$ of mass M floating on top of the water surface, called buoy in the following. A general planar movement supposes three degrees of freedom, in the following denoted χ, ζ and θ, see Figure 1. The buoy is supposed not to touch the bottom. The interior unit normal to the buoy surface is denoted by n and its center of mass $G = (\chi, \zeta)$, where $\chi \in \Omega_x$ denotes the horizontal and $\zeta \in \mathbb{R}$ the vertical component. The variable θ stands for the angle between the unit vector in the vertical direction e_z and the vector GX where X is a point in the solid different from the center of mass. The moment of inertia of the solid around an axis passing through the center of mass is denoted $\mathcal{J}_G$.

A general planar motion of a rigid body can be separated into a translational motion of a point in the body and a rotational motion around an axis through that point. The most convenient, in most cases, is to choose this point as the center of mass G. In the part of the domain where there is no buoy, the roof is defined high enough not to touch the fluid surface and otherwise the roof is given by

$$R(x,t) = \mathcal{R}(x, \chi(t), \zeta(t), \theta(t)) \tag{3}$$

where

$$\mathcal{R}(x,\chi,\zeta,\theta) = R_0(x-\chi,\theta) + \zeta \tag{4}$$

with $R_0(x,\theta)$ a continuum characterizing the geometry of the inferior surface of the floating object at position $x \in \Omega_x$ and for any angle $\theta \in [-\pi,\pi]$. For a discal buoy with radius r, an expression can be given for R_0. Since the geometry is independent of the rotation, it writes $R_0(x,\theta) = -\sqrt{r^2-x^2}$. For an elliptical buoy with semi-minor and semi-major axis respectively equal to a and b, $R_0(x,\theta)$ is the lower root of the second order polynomial $\mathcal{P}(z) = \dfrac{(x\cos\theta + z\sin\theta)^2}{a^2} + \dfrac{(x\sin\theta - z\cos\theta)^2}{b^2} - 1$. Since the function R_0 is not always explicit, we will explain in Section 3.4 the numerical handling.

The horizontal (resp. vertical) forces other than the weight and the pressure from the fluid will be denoted by F_χ (resp. F_ζ). Their torque around the center of mass is denoted by T_θ. These forces could for example represent a mooring line and do not play a direct role in the interaction between the fluid and the solid.

Proposition 1. *A general planar movement of the solid body $\mathcal{B}$ is described by the system*

$$\begin{cases} M\ddot{\chi} = -\displaystyle\int_{\Omega_x} p_\eta \partial_x \mathcal{R} \mathrm{d}x + F_\chi \\ M\ddot{\zeta} = -Mg + \displaystyle\int_{\Omega_x} p_\eta \mathrm{d}x + F_\zeta \\ \mathcal{J}_G\ddot{\theta} = \displaystyle\int_{\Omega_x} p_\eta \partial_\theta \mathcal{R} \mathrm{d}x + T_\theta \end{cases} \tag{5}$$

completed with the initial conditions $\chi(0) = \chi^0$, $\dot{\chi}(0) = \dot{\chi}^0$, $\zeta(0) = \zeta^0$, $\dot{\zeta}(0) = \dot{\zeta}^0$, $\theta(0) = \theta^0$ and $\dot{\theta}(0) = \dot{\theta}^0$.

Proof. The translational motion can be described by Newton's second law of motion. Taking into account the forces F_χ, F_ζ, the weight together with the pressure applied on the buoy from the water gives the following equations

$$\begin{cases} M\ddot{\chi} = \displaystyle\int_{\Omega_x} p_\eta n \cdot e_x \sqrt{1+(\partial_x\mathcal{R})^2}\mathrm{d}x + F_\chi \\ M\ddot{\zeta} = -Mg + \displaystyle\int_{\Omega_x} p_\eta n \cdot e_z \sqrt{1+(\partial_x\mathcal{R})^2}\mathrm{d}x + F_\zeta. \end{cases} \tag{6}$$

The rotational movement is described by the angular momentum theorem, i.e.

$$\partial_t \mathcal{L}_G = \int_{\Omega_x} p_\eta (GX \times n) \cdot e_y \sqrt{1+(\partial_x\mathcal{R})^2}\mathrm{d}x + T_\theta \tag{7}$$

where $\mathcal{L}_G$ denotes the angular momentum around G, X a point at the surface with coordinates $(X_x, \mathcal{R}(X_x,\chi,\zeta,\theta))$ and $e_y = e_x \times e_z$ the unit vector in the direction perpendicular to the plane.

By definition, in a planar framework $\partial_t \mathcal{L}_G = \mathcal{J}_G \ddot{\theta}$.

Replacing the interior normal $n = \dfrac{1}{\sqrt{1+(\partial_x \mathcal{R})^2}} \begin{pmatrix} -\partial_x \mathcal{R} \\ 1 \end{pmatrix}$ in (6) leads to the first two equations of (5) and for (7) it yields

$$\mathcal{J}_G \ddot{\theta} = -\int_{\Omega_x} p_\eta \left(GX \cdot e_z \partial_x \mathcal{R} + GX \cdot e_x \right) \mathrm{d}x + T_\theta. \tag{8}$$

In the reference frame of the center of mass denoted by $\widetilde{\ }$, the movement is a simple rotation of angle θ and as a consequence the coordinates $\left(\widetilde{X}_x, \widetilde{\mathcal{R}}\left(\widetilde{X}_x, \theta\right)\right)$ of the point X verify

$$\begin{pmatrix} \widetilde{X}_x \\ \widetilde{\mathcal{R}} \end{pmatrix} = \begin{pmatrix} \cos\left(\theta - \theta^0\right) & \sin\left(\theta - \theta^0\right) \\ -\sin\left(\theta - \theta^0\right) & \cos\left(\theta - \theta^0\right) \end{pmatrix} \begin{pmatrix} \widetilde{X}_x^0 \\ \widetilde{\mathcal{R}}\left(\widetilde{X}_x^0, \theta^0\right) \end{pmatrix}$$

with $\left(\widetilde{X}_x^0, \widetilde{\mathcal{R}}\left(\widetilde{X}_x^0, \theta^0\right)\right)$ the coordinates of the point X with an angle θ^0.
The previous relation implies

$$\widetilde{\mathcal{R}} = \partial_\theta \widetilde{X}_x. \tag{9}$$

Moreover the trajectory of the points of the buoy are concentric circles, i.e. $\partial_\theta \|GX\| = 0$. Thus

$$\partial_\theta \left(\left(\widetilde{X}_x\right)^2 + \left(\widetilde{\mathcal{R}}\left(\widetilde{X}_x, \theta\right)\right)^2 \right) = 0$$

and it follows

$$\widetilde{X}_x \partial_\theta \widetilde{X}_x + \widetilde{\mathcal{R}} \partial_\theta \widetilde{X}_x \partial_x \widetilde{\mathcal{R}} + \widetilde{\mathcal{R}} \partial_\theta \widetilde{\mathcal{R}} = 0.$$

Using now the relation (9), we get

$$\widetilde{X}_x + \widetilde{\mathcal{R}} \partial_x \widetilde{\mathcal{R}} + \partial_\theta \widetilde{\mathcal{R}} = 0.$$

Finally introducing this relation in (8) and noticing that $GX \cdot e_z = \widetilde{\mathcal{R}}$ and $GX \cdot e_x = \widetilde{X}_x$ gives the last equation in (5). □

The solid system admits the following energy balance law.

Lemma 2.2. *Any smooth solution of (5) satisfies the following energy law*

$$\partial_t E = \left(\int_{\Omega_x} p_\eta \mathrm{d}x + F_\zeta \right) \dot{\zeta} - \left(\int_{\Omega_x} p_\eta \partial_x \mathcal{R} \ \mathrm{d}x - F_\chi \right) \dot{\chi} + \left(\int_{\Omega_x} p_\eta \partial_\theta \mathcal{R} \mathrm{d}x + T_\theta \right) \dot{\theta}$$

with $E\left(\chi, \zeta, \theta\right) = \dfrac{M}{2}\left(\dot{\zeta}^2 + \dot{\chi}^2\right) + \dfrac{\mathcal{J}_G}{2}\dot{\theta}^2 + Mg\zeta.$

Proof. Multiplying the first equation of (5) by $\dot{\chi}$, the second equation by $\dot{\zeta}$, the third equation by $\dot{\theta}$ and summing gives the result. □

An energy law for the coupled fluid-solid system (5) and (1)-(2) is obtained.

Proposition 2. *Considering a no-flux boundary on Ω_x, any smooth solution of (5) and (1)-(2) satisfies the following energy balance law*

$$\partial_t \left(\int_{\Omega_x} \mathcal{E} \ \mathrm{d}x + E \right) = \int_{\Omega_x} \left(gh + p_\eta \right) \partial_t B \mathrm{d}x + F_\zeta \dot{\zeta} + F_\chi \dot{\chi} + T_\theta \dot{\theta}.$$

Proof. It follows from (3)-(4) that

$$\begin{aligned}\partial_t R(x,t) &= \dot{\chi}\partial_\chi \mathcal{R}(x,\chi,\zeta,\theta) + \dot{\zeta}\partial_\zeta \mathcal{R}(x,\chi,\zeta,\theta) + \dot{\theta}\partial_\theta \mathcal{R}(x,\chi,\zeta,\theta) \\ &= -\dot{\chi}\partial_x \mathcal{R}(x,\chi,\zeta,\theta) + \dot{\zeta} + \dot{\theta}\partial_\theta \mathcal{R}(x,\chi,\zeta,\theta).\end{aligned} \tag{10}$$

Now integrating the energy balance law from Lemma 2.1 over Ω_x and summing with the result from Lemma 2.2 concludes the proof. □

3. Numerical resolution

This section is devoted to the numerical resolution of (1)-(2) and (5).

3.1. **Discretization for the fluid dynamics.** Let us firstly remind some properties of the numerical strategy proposed in [12] for the congested shallow water model (1)-(2).
Let $\mathbb{T}$ be a mesh of Ω_x composed of control volumes. We denote $k \in \mathbb{T}$ a control volume, x_k the coordinate of its center and by the subscript $k-\frac{1}{2}$ (resp. $k+\frac{1}{2}$) its left (resp. right) face. The space step is defined by $|k|$. In addition the time step is denoted by δ_t^{n+1}, i.e. $t^{n+1} = t^n + \delta_t^{n+1}$.
The mean bottom level in the control volume k, at time t^n, is denoted by B_k^n.

A pseudo-compressibility method is used to take into account the congestion constraint. Let us denote by λ the relaxation parameter.
Following [12], one particularity of the proposed scheme is that the numerical unknowns are ϕ_k^n and $\overline{u}_k^n$ which are the average of the potential defined by $\phi = g(h+B) + p_\eta$ and the velocity $\overline{u}$ in the volume k at time t^n. The potential can be used as a parametrization of the water depth and the surface pressure, thus we set

$$h(k,n;\phi) = \begin{cases} \dfrac{\phi}{g} - B_k^n, & \text{if } \phi \le gR_k^n \\ \dfrac{R_k^n - B_k^n + \lambda^2\left(\frac{\phi}{g} - B_k^n\right)}{1+\lambda^2}, & \text{else} \end{cases}$$

and

$$p(k,n;\phi) = \phi - g\left(h(k,n;\phi) + B_k^n\right)$$

where R_k^n is an approximation of the mean value of the roof level in the control volume k at time t^n. For readability, we set $h_k^n = h(k,n;\phi_k^n)$ and $p_k^n = p(k,n;\phi_k^n)$. We also introduce the following notation

$$\partial_t^{n+1}\psi = \frac{\psi^{n+1} - \psi^n}{\delta_t^{n+1}}.$$

The scheme finally reads

$$h_k^{n+1} = h_k^n - \frac{\delta_t^{n+1}}{|k|}\left(\mathcal{F}_{k+\frac{1}{2}}^{n+1} - \mathcal{F}_{k-\frac{1}{2}}^{n+1}\right) \tag{11}$$

and

$$\begin{aligned} h_k^{n+1}\overline{u}_k^{n+1} &= h_k^n\overline{u}_k^n - \delta_t^{n+1}h_k^{n+1}\frac{\phi_{k+1}^{n+1} - \phi_{k-1}^{n+1}}{2|k|} \\ &\quad - \frac{\delta_t^{n+1}}{|k|}\left(\overline{u}_k^n\left(\mathcal{F}_{k+\frac{1}{2}}^{n+1}\right)_+ - \overline{u}_{k+1}^n\left(\mathcal{F}_{k+\frac{1}{2}}^{n+1}\right)_- + \overline{u}_k^n\left(\mathcal{F}_{k-\frac{1}{2}}^{n+1}\right)_- - \overline{u}_{k-1}^n\left(\mathcal{F}_{k-\frac{1}{2}}^{n+1}\right)_+\right)\end{aligned} \tag{12}$$

with $\mathcal{F}^{n+1}_{k+\frac{1}{2}}$ an approximation of the mean mass flux $h\overline{u}$ at the face $k+\frac{1}{2}$ between the times t^n and t^{n+1}. More precisely

$$\mathcal{F}^{n+1}_{k+\frac{1}{2}} = \frac{h^{n+1}_k \overline{u}^n_k + h^{n+1}_{k+1}\overline{u}^n_{k+1}}{2} - \frac{\gamma \delta_t^{n+1}}{2}\left(\frac{h^{n+1}_k}{|k|} + \frac{h^{n+1}_{k+1}}{|k+1|}\right)\frac{\left(\phi^{n+1}_{k+1} - \phi^{n+1}_k\right)}{2} \tag{13}$$

with a regularization parameter $\gamma \geq 0$ characteristic of the scheme, see [25]. The numerical scheme requires boundary conditions which depend on the regime of the flow. In the current work, we do not detail the boundary conditions treatment, see [22, section 21.8] for more details.
The following energy dissipation law has been proven in [12, Proposition 2.3].

Lemma 3.1. *For any $\gamma \geq 1$ and under the CFL condition*

$$\left(\left|\frac{\overline{u}^n_k + \overline{u}^n_{k+1}}{2}\right| + \sqrt{\frac{\gamma}{2}}\sqrt{\left|\frac{\phi^{n+1}_{k+1} - \phi^{n+1}_k}{2}\right|}\right)\delta_t^{n+1} \leq \frac{\min\left(h^{n+1}_k, h^{n+1}_{k+1}\right)}{2\left(h^{n+1}_k + h^{n+1}_{k+1}\right)}\min\left(|k|, |k+1|\right) \tag{14}$$

there exists a discrete flux $\mathcal{G}^{n+1}_{k+\frac{1}{2}}$ such that the scheme (11)-(13) admits the following energy dissipation law

$$\partial_t^{n+1}\mathcal{E}_k + \frac{1}{|k|}\left(\mathcal{G}^{n+1}_{k+\frac{1}{2}} - \mathcal{G}^{n+1}_{k-\frac{1}{2}}\right) \leq -p^{n+1}_k \partial_t^{n+1} R_k + \left(g h^n_k + p^{n+1}_k\right)\partial_t^{n+1} B_k \tag{15}$$

with the discrete mechanical energy

$$\mathcal{E}^n_k = \frac{1}{2}h^n_k\left(\overline{u}^n_k\right)^2 + g h^n_k\left(B^n_k + \frac{h^n_k}{2}\right) + \frac{g}{2\lambda^2}\left(h^n_k - R^n_k + B^n_k\right)^2_+$$

and $\mathcal{G}^{n+1}_{k+\frac{1}{2}}$ defined in [12].

Note that in the present work, R^n_k depends on the values χ^n, ζ^n and θ^n via (4). In the next section, the numerical resolution for the latter and its coupling with the fluid scheme will be detailed.

3.2. **Discretization for the solid dynamics.** The three degrees of freedom of the solid at time t^n are respectively denoted by θ^n, χ^n and ζ^n.

Due to its simple implementation, a Newmark scheme is chosen to solve the buoy dynamics (5). In fact each time step only requires the resolution of one set of equations. For $(\alpha, \beta) \in [0,1]^2$, the Newmark scheme for an ODE of the form $\ddot{\Lambda} = \mathcal{H}\left(\Lambda, \dot{\Lambda}, t\right)$ writes

$$\begin{cases} \Lambda^{n+1} = \Lambda^n + \delta_t^{n+1}\dot{\Lambda}^n + \dfrac{\left(\delta_t^{n+1}\right)^2}{2}\left(\beta\ddot{\Lambda}^{n+1} + (1-\beta)\ddot{\Lambda}^n\right) \\ \dot{\Lambda}^{n+1} = \dot{\Lambda}^n + \delta_t^{n+1}\left(\alpha\ddot{\Lambda}^{n+1} + (1-\alpha)\ddot{\Lambda}^n\right) \end{cases} \tag{16}$$

where in our case $\Lambda = \begin{pmatrix} \chi \\ \zeta \\ \theta \end{pmatrix}$ and $\mathcal{H}$ is given in (5).

For the approximation of the integrals in (5) we take

$$\begin{cases} M\ddot{\chi}^n = -\sum_{k\in\mathbb{T}} |k| p_k^n \partial_k^\delta R^n + F_\chi^n & (17) \\ M\ddot{\zeta}^n = -Mg + \sum_{k\in\mathbb{T}} |k| p_k^n + F_\zeta^n & (18) \\ \mathcal{J}_G \ddot{\theta}^n = \sum_{k\in\mathbb{T}} |k| p_k^n \partial_\theta^\delta R_k^n + T_\theta^n & (19) \end{cases}$$

where $\partial_k^\delta R^n$ (resp. $\partial_\theta^\delta R_k^n$) are discretizations of the derivative of the roof with respect to x (resp. θ) at time t^n. These terms will be discussed below in order to obtain the energy stability for the coupled fluid-solid model. Let us first state the energy stability for the Newmark scheme.

Lemma 3.2. *Let $\alpha = \beta = 1$. Then the scheme (16)-(19) satisfies the following energy law*

$$\begin{aligned} \partial_t^{n+1} E \quad = \quad & -\left(\sum_{k\in\mathbb{T}} \left(|k| \partial_k^\delta R^{n+1} p_k^{n+1} \right) - F_\chi^{n+1} \right) \partial_t^{n+1} \chi \\ & + \left(\sum_{k\in\mathbb{T}} \left(|k| p_k^{n+1} \right) + F_\zeta^{n+1} \right) \partial_t^{n+1} \zeta \\ & + \left(\sum_{k\in\mathbb{T}} \left(|k| \partial_\theta^\delta R_k^{n+1} p_k^{n+1} \right) + T_\theta^{n+1} \right) \partial_t^{n+1} \theta \end{aligned} \tag{20}$$

with $E^n = E\left(\chi^n, \zeta^n, \theta^n\right)$ defined in Lemma 2.2.

Proof. Let $\alpha = \beta = 1$. The proof for the general ODE case is detailed in [19, section 3]. Using a Newmark scheme for the linear equation of motion on a vector of unknowns Λ

$$C_1 \ddot{\Lambda}^n + C_2 \dot{\Lambda}^n + C_3 \Lambda^n = f^n \tag{21}$$

where C_1, C_2 and C_3 are matrices and f a vector representing the external forces, the author proves the following energy equation

$$\begin{aligned} \partial_t^{n+1} \left(\frac{1}{2} \dot{\Lambda} \cdot \left(C_1 + \frac{\delta_t^{n+1}}{2} C_2 \right) \dot{\Lambda} + \frac{1}{2} \Lambda \cdot C_3 \Lambda \right) = & -\frac{\delta_t^{n+1}}{2} \partial_t^{n+1} \Lambda \cdot C_3 \partial_t^{n+1} \Lambda \\ & + \partial_t^{n+1} \Lambda \cdot \left(\frac{1}{2} \left(f^{n+1} + f^n \right) + \frac{\delta_t^{n+1}}{2} \partial_t^{n+1} f \right) \\ & - \frac{1}{2} \left(\partial_t^{n+1} \Lambda \cdot C_2 \partial_t^{n+1} \Lambda \right) - \frac{1}{2} \left(\frac{\dot{\Lambda}^{n+1} + \dot{\Lambda}^n}{2} \cdot C_2 \frac{\dot{\Lambda}^{n+1} + \dot{\Lambda}^n}{2} \right). \end{aligned}$$

Applied in our case by setting $C_1 = \begin{pmatrix} M & 0 & 0 \\ 0 & M & 0 \\ 0 & 0 & \mathcal{J}_G \end{pmatrix}$, $C_2 = 0$, $C_3 = 0$ and $f^n = \begin{pmatrix} -\sum_{k\in\mathbb{T}} |k| p_k^n \partial_k^\delta R^n + F_\chi^n \\ -Mg + \sum_{k\in\mathbb{T}} |k| p_k^n + F_\zeta^n \\ \sum_{k\in\mathbb{T}} |k| p_k^n \partial_\theta^\delta R_k^n + T_\theta^n \end{pmatrix}$, we conclude since we have $\partial_t^{n+1} E = \partial_t^{n+1}\left(\frac{1}{2}\dot{\Lambda}\cdot C_1\dot{\Lambda}\right) + Mg\partial_t^{n+1}\zeta$. □

Note that by taking $\alpha = \beta = 1$, the Newmark scheme is completely implicit and of first order.

3.3. **Coupling strategy between the fluid and the solid.** Let us now concentrate on the discrete coupling. We will discuss the form of $\partial_k^\delta R^n$ and $\partial_\theta^\delta R_k^n$ in (17)-(19) and analyze the energy of the coupled system. A first naive approach that is not entropy satisfying will be given. In a second paragraph an adapted choice for $\partial_k^\delta R^n$ and $\partial_\theta^\delta R_k^n$ will be explained. It is introduced in order to obtain an energy dissipation law.

3.3.1. *A first approach.* In this section a straightforward discretization for $\partial_k^\delta R^n$ and $\partial_\theta^\delta R_k^n$ is analyzed. We take $\partial_k^\delta R^n = \partial_k^C R^n$ and $\partial_\theta^\delta R_k^n = \partial_\theta^C R_k^n$ in (17)-(19), where

$$\partial_k^C R^n = \frac{R_{k+1}^{n-1} - R_{k-1}^{n-1}}{2|k|} \qquad \text{and} \qquad \partial_\theta^C R_k^n = -\widetilde{R}_k^{n-1}\partial_k^C R^n - \widetilde{X}_k^{n-1} \tag{22}$$

with $\widetilde{X}_k^n = x_k - \chi^n$ and $\widetilde{R}_k^n = R_k^n - \zeta^n$. The choice for $\partial_k^C R^n$ is a centered discretization of $\partial_x \mathcal{R}$ and the discretization of $\partial_\theta^C R_k^n$ comes from (8). More precisely $\partial_\theta^C R_k^n$ is a discretization of $-GX\cdot e_z \partial_x \mathcal{R} - GX\cdot e_x$.
A discrete energy inequality for the coupled fluid-solid system can be written.

Lemma 3.3. *Consider a no-flux boundary on Ω_x and let $\alpha = \beta = 1$. Then the scheme (11)-(13) and (16)-(19) with (22) admits the following energy inequality*

$$\begin{aligned} \partial_t^{n+1}\left(\sum_{k\in\mathbb{T}} |k|\mathcal{E}_k + E\right) \le \sum_{k\in\mathbb{T}} \left(|k|\left(gh_k^n + p_k^{n+1}\right)\partial_t^{n+1} B_k\right) \\ + F_\zeta^{n+1}\partial_t^{n+1}\zeta - F_\chi^{n+1}\partial_t^{n+1}\chi + T_\theta^{n+1}\partial_t^{n+1}\theta \\ + \sum_{k\in\mathbb{T}} |k| p_k^{n+1}\left(-\partial_t^{n+1} R_k - \partial_t^{n+1}\chi\partial_k^\delta R^{n+1} + \partial_t^{n+1}\zeta + \partial_t^{n+1}\theta\partial_\theta^\delta R_k^{n+1}\right). \end{aligned} \tag{23}$$

Proof. Summing (15) over the computational domain and adding (20) gives the result. □

Except for the last sum, the energy inequality (23) is consistent with the energy given in Proposition 2. Since we do not have an equivalent condition to (10) at the discrete level, the last sum in (23) does not vanish and its sign cannot be determined. As a consequence no energy stability is obtained. However a simple choice of discretization for $\partial_k^\delta R^n$ and $\partial_\theta^\delta R_k^n$ can be made to get an energy balance law for the system at the discrete level. This will be explained in the next section.

3.3.2. *Entropy correction.* Let us now discuss a choice for $\partial_k^\delta R^n$ and $\partial_\theta^\delta R_k^n$ such that the energy stability is ensured. Let

$$\partial_k^\delta R^n = \begin{cases} \dfrac{\partial_t^n \zeta - \partial_t^n R_k}{\partial_t^n \chi}, & \text{if } \partial_t^n \chi \neq 0 \text{ and } \partial_t^n \theta = 0 \\ \partial_k^C R^n, & \text{else} \end{cases} \tag{24}$$

and

$$\partial_\theta^\delta R_k^n = \begin{cases} \dfrac{\partial_t^n R_k + \partial_t^n \chi \partial_k^C R^n - \partial_t^n \zeta}{\partial_t^n \theta}, & \text{if } \partial_t^n \theta \neq 0 \\ \partial_\theta^C R_k^n, & \text{else.} \end{cases} \tag{25}$$

For (24)-(25) to be numerically well defined when $\partial_t^n \chi \to 0$ (resp. $\partial_t^n \theta \to 0$) a tolerance is introduced in practice, see Section 3.4. With the previous choice, an energy dissipation law can be proven.

Proposition 3. *Consider a no-flux boundary on Ω_x and let $\alpha = \beta = 1$, then the scheme (11)-(13) and (16)-(19) with (24)-(25) admits the following dissipation law*

$$\partial_t^{n+1}\left(\sum_{k\in\mathbb{T}} |k|\mathcal{E}_k + E\right) \leq \sum_{k\in\mathbb{T}} \left(|k|\left(gh_k^n + p_k^{n+1}\right)\partial_t^{n+1} B_k\right) + F_\zeta^{n+1}\partial_t^{n+1}\zeta - F_\chi^{n+1}\partial_t^{n+1}\chi + T_\theta^{n+1}\partial_t^{n+1}\theta.$$

Proof. Following the inequality of Lemma 3.3, it is sufficient to prove that

$$-\partial_t^{n+1} R_k - \partial_t^{n+1}\chi \partial_k^\delta R^{n+1} + \partial_t^{n+1}\zeta + \partial_t^{n+1}\theta \partial_\theta^\delta R_k^{n+1} = 0. \tag{26}$$

Replacing the expressions of $\partial_k^\delta R^n$ and $\partial_\theta^\delta R_k^n$ from (24)-(25) in (26) concludes the proof. □

The choice (24)-(25) is made to impose (10) at the discrete level. The consistency of (24)-(25) with the respective derivative is therefore straightforward. If $\partial_t^n \chi = 0$ and $\partial_t^n \theta = 0$ there is no condition to verify and any choice can be made for $\partial_k^\delta R^n$ and $\partial_\theta^\delta R_k^n$. In the case where $\partial_t^n \theta = 0$ or $\partial_t^n \chi = 0$, a condition on $\partial_\theta^\delta R_k^n$ (resp. $\partial_k^\delta R^n$) is obtained to verify (10) at the discrete level. In the last case, i.e. $\partial_t^n \chi \neq 0$ and $\partial_t^n \theta \neq 0$, a condition is imposed on $\partial_\theta^\delta R_k^n$, i.e. $\partial_\theta^\delta R_k^n = \dfrac{\partial_t^n R_k + \partial_t^n \chi \partial_k^\delta R^n - \partial_t^n \zeta}{\partial_t^n \theta}$ and any discretization for $\partial_k^\delta R^n$ can be chosen.

3.4. **Practical details.** Some details about the practical implementation are given below.

Correction near equilibrium. For (24)-(25) to be numerically well defined when $\partial_t^n \chi \to 0$ (resp. $\partial_t^n \theta \to 0$), a tolerance $\varepsilon_t > 0$ is introduced in practice, i.e.

$$\partial_k^\delta R^n = \begin{cases} \dfrac{\partial_t^n \zeta + \partial_t^n \theta \partial_\theta^C R_k^n - \partial_t^n R_k}{\partial_t^n \chi}, & \text{if } |\chi^{n+1} - \chi^n| > \varepsilon_t \text{ and } |\theta^{n+1} - \theta^n| < \varepsilon_t \\ \partial_k^C R^n, & \text{else} \end{cases} \tag{27}$$

and

$$\partial_\theta^\delta R_k^n = \begin{cases} \dfrac{\partial_t^n R_k + \partial_t^n \chi \partial_k^C R^n - \partial_t^n \zeta}{\partial_t^n \theta}, & \text{if } |\theta^{n+1} - \theta^n| > \varepsilon_t \\ \partial_\theta^C R_k^n, & \text{else.} \end{cases} \tag{28}$$

Considering a no-flux boundary on Ω_x as well as a smooth enough roof and letting $\alpha = \beta = 1$, there exists $\Xi \in \mathbb{R}$ such that the scheme (11)-(13) and (16)-(19) with (27)-(28) admits the following energy inequality

$$\begin{aligned} \partial_t^{n+1} \left(\sum_{k \in \mathbb{T}} |k| \mathcal{E}_k + E \right) \quad \leq \quad & \sum_{k \in \mathbb{T}} \left(|k| \left(p_k^{n+1} + g h_k^n \right) \partial_t^{n+1} B_k \right) \\ & + F_\zeta^{n+1} \partial_t^{n+1} \zeta - F_\chi^{n+1} \partial_t^{n+1} \chi + T_\theta^{n+1} \partial_t^{n+1} \theta \\ & + \Xi \, \varepsilon_t. \end{aligned}$$

In the considered applications, the buoy is supposed smooth enough and is moving, i.e. $|\theta^{n+1} - \theta^n| > \varepsilon_t$ or $|\chi^{n+1} - \chi^n| > \varepsilon_t$. Thus the energy between the solid and the fluid is perfectly controlled. Close to the equilibrium, i.e. $|\theta^{n+1} - \theta^n| < \varepsilon_t$ and $|\chi^{n+1} - \chi^n| < \varepsilon_t$, the energy is not perfectly preserved, but is bounded by an arbitrary small parameter.

Fixed point approach. The scheme (11)-(13) is implicit and non-linear on the potential. An iterative Newton process on the potential is explained in [12] to solve it at each time step. The fixed point resolution has to be adapted to take into account the dynamics of the buoy. More precisely the iterations will be done on the variable $W^n = (\phi^n, \Lambda^n)$.
The derivatives of the water height with respect to χ, ζ and θ depend on the shape of the buoy which makes the Jacobian difficult to be computed. Therefore a semi-Newton fixed point is implemented, for which the latter derivatives are not taken into account. As a consequence no quadratic convergence is recovered.
Two stopping criteria are used to increase the reliability of the result. If the L^∞-norm of the residual and $\|W^{n,q+1} - W^{n,q}\|_\infty$ are inferior to a tolerance ε_{Newton}, we set $W^{n+1} = W^{n,q+1}$.
A large time step given by (14) which takes into account only the fluid is not necessarily adapted to the induced large buoy movement and can result in a large number of fixed point iterations. To avoid two-way wiring in the fixed point, the time step is limited if necessary, see for example [8] for time step adaptation in a fixed point method. We set a maximum acceptable number of iterations i_{max} in the fixed point. If the Newton fixed point takes too many iterations to converge, the time step is reduced, i.e. $\delta_t^{n,q+1} = \omega \delta_t^{n,q}$ with $\omega < 1$ and the time iteration is recomputed, i.e. $W^{n,q+1} = W^n$.
The implicit CFL condition (14) is verified for every time iteration at convergence to ensure the scheme to be entropy satisfying, see Lemma 3.1. If the CFL condition is not verified, the time step is recomputed using the new time step.
In practice the fixed point algorithm converges in a few iterations with reasonable time steps. The performance of the fixed point will be given for each test case done below. A rigourous proof of convergence for the fixed point has not been done in this work.

Buoy implementation. Let us explain the implementation of the geometry of the buoy, since an explicit expression of R_0 is not easy to have, even for a simple geometry.
In practice a finite set of points $\mathcal{S} = \{(x, z) \mid x \in \mathcal{S}_x,\ z \in \mathcal{S}_z\} \subset \Omega_x \times \mathbb{R}$ describing the geometry is given.
For any point x_k not under the buoy, the roof is defined high enough not to touch the fluid surface.
In the part of the domain where the buoy is, the roof is deduced from $\mathcal{S}$. For $x_k \in \Omega_x$, let $x_k^- = \max\{x \in \mathcal{S}_x |\ x \leq x_k\}$ and $x_k^+ = \min\{x \in \mathcal{S}_x |\ x_k \leq x\}$. In other words, x_k^- (resp. x_k^+) is the nearest abscissa from the left (respectively from the right) to x_k among the set of points $\mathcal{S}$. We set $z_k^- = \min\{z |\ (x_k^-, z) \in \mathcal{S}\}$ and $z_k^+ = \min\{z |\ (x_k^+, z) \in \mathcal{S}\}$. To get an approximation of the roof in x_k a linear interpolation between the coordinates of the two points (x_k^-, z_k^-) and (x_k^+, z_k^+) is done.

4. Simulations

Simulations in a one dimensional framework are shown.
A first test case is the return to equilibrium problem. A reference solution is given in [20] through the resolution of a nonlinear ODE. The simulation is compared to this reference solution.
In order to show the robustness of the code, a second test case where a structure with initial velocity is falling into water at rest is proposed.
The last test case shows the ability to simulate wave energy converters.

In the following we take $g = 9.81$. The length of the domain Ω_x and the final time of simulation are respectively denoted by l and $\mathcal{T}$. The space step using a regular grid is denoted by δ_x. The relaxation parameter is chosen as $\lambda = \sqrt{\delta_x}$, see [12] for more details about this choice. The CPR-parameter γ is set to 2. It is slightly increased compared to the optimal value necessary to get the entropy in Lemma 3.1. This allows to get more regularization, see [25]. Otherwise oscillations in the vicinity of a shock due to oscillation effects of the CPR scheme can be observed. For all the test cases $\varepsilon_{Newton} = 1 \times 10^{-8}$, $i_{max} = 15$, $\varepsilon_t = \varepsilon_{Newton}$ and $\omega = \frac{1}{4}$.

4.1. **Return to equilibrium.**

To validate our method, the simulation will be confronted with a reference solution given in [20] and the order of convergence will be computed.

Only a vertical movement is considered for this test case. More precisely we suppose that

$$F_\chi = \int_{\Omega_x} p_\eta \partial_x \mathcal{R}\, \mathrm{d}x, \qquad T_\theta = -\int_{\Omega_x} p_\eta \partial_\theta \mathcal{R}\, \mathrm{d}x \qquad \text{and} \qquad F_\zeta = 0 \tag{29}$$

which expresses the fact that the horizontal and angular degrees of freedom are fixed.

An analytical solution was proposed in [20, Corollary 1] for the return to the equilibrium case. It corresponds to the movement of an object initially at rest and with the water at rest, starting from a configuration where it is not at its equilibrium position denoted by ζ_{eq} and evolving towards it. The equilibrium of the buoy is

defined by $u = 0$, $\phi = \phi_0 \in \mathbb{R}$, $\dot{\zeta} = 0$ and $\zeta = \zeta_{eq}$ such that

$$Mg = \int_{\Omega_x} p_\eta \, \mathrm{d}x. \tag{30}$$

In other words the equilibrium is the situation where the surface pressure balances out the weight of the buoy.

We define $\delta_G = \zeta - \zeta_{eq}$ the distance of the center of mass to the equilibrium position with the initial conditions $\delta_G^0 = \zeta^0 - \zeta_{eq}$ and $\dot{\delta_G^0} = \dot{\zeta}^0$. The water height corresponding to the equilibrium position is denoted h_{eq}. A rectangular buoy is considered which corresponds to a flat roof. The length of the roof is equal to $l_R = 0.8$ and defined so that it is symmetric with respect to its center of mass. A flat bottom is considered for simplicity. For the above defined configuration, the position of the center of mass is determined by

$$\left(M + \frac{2}{3\zeta} \left(\frac{l_R}{2} \right)^3 \right) \ddot{\delta_G} = -g l_R \delta_G - \nu \left(\dot{\delta_G} \right) + \mu \left(\delta_G \right) \dot{\delta_G}^2 \tag{31}$$

with the coefficients

$$\nu \left(\dot{\delta_G} \right) = g l_R \left(h_{eq} - \tau \left(\frac{l_R}{4\sqrt{g}} \dot{\delta_G} \right)^2 \right)$$

and

$$\mu \left(\delta_G \right) = \frac{4}{3\zeta^2} \left(\left(\frac{l_R}{2} - \chi^0 \right)^3 + \left(\chi^0 \right)^3 \right).$$

The coefficient τ is given by

$$\tau \left(r \right) = \frac{1}{3} \left(\sqrt{h_{eq}} + C \left(r \right) + \frac{h_{eq}}{C \left(r \right)} \right)$$

with

$$C \left(r \right) = \frac{3}{2} \left(-4r + \frac{8}{27} h_{eq}^{\frac{3}{2}} + 4 \sqrt{r \left(r - \frac{4}{27} h_{eq}^{\frac{3}{2}} \right)} \right)^{\frac{1}{3}}.$$

The simulation is done in a domain of length $l = 40$. The final time $\mathcal{T}$ is equal to 4 and the mass $M = 0.5$. We consider an equilibrium with $\zeta_{eq} = 1$ and the water depth h_{eq} satisfying (30). The initial conditions read $\phi^0 = g h_{eq}$ and $\overline{u}^0 = 0$. Initially the position of the center of mass is $\chi^0 = 20$, $\zeta^0 = 1.2$ and $\theta^0 = 0$ and it has a null velocity. The initial position is above the equilibrium position.

The simulation is compared to the reference solution in Figure 2. More precisely the evolution in time of the distance to the equilibrium position is shown. The agreement between the two solutions is good and the solution tends to the equilibrium position as expected. The convergence rate in L^2-norm for δ_G is shown in Figure 3. The error computed corresponds to the L^2-norm of the difference between the 'exact' (obtained by solving the ODE (31)) and the computed position of the center of mass over the time interval $[0, 4]$. A slightly better than first order convergence is obtained. By taking $\alpha = \beta = 1$, the Newmark scheme is completely implicit and therefore of first order.

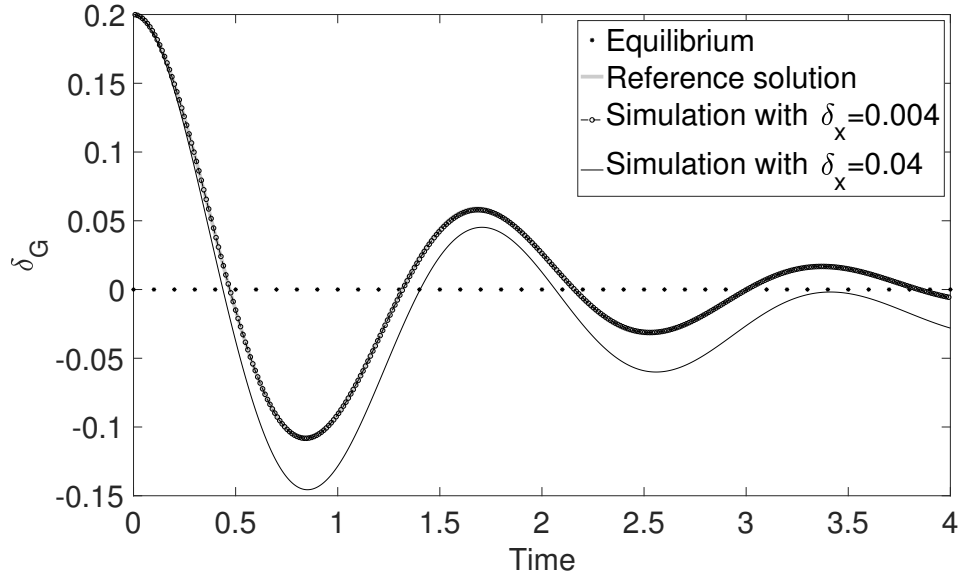

FIGURE 2. Return to equilibrium: evolution of the distance to the equilibrium position in time

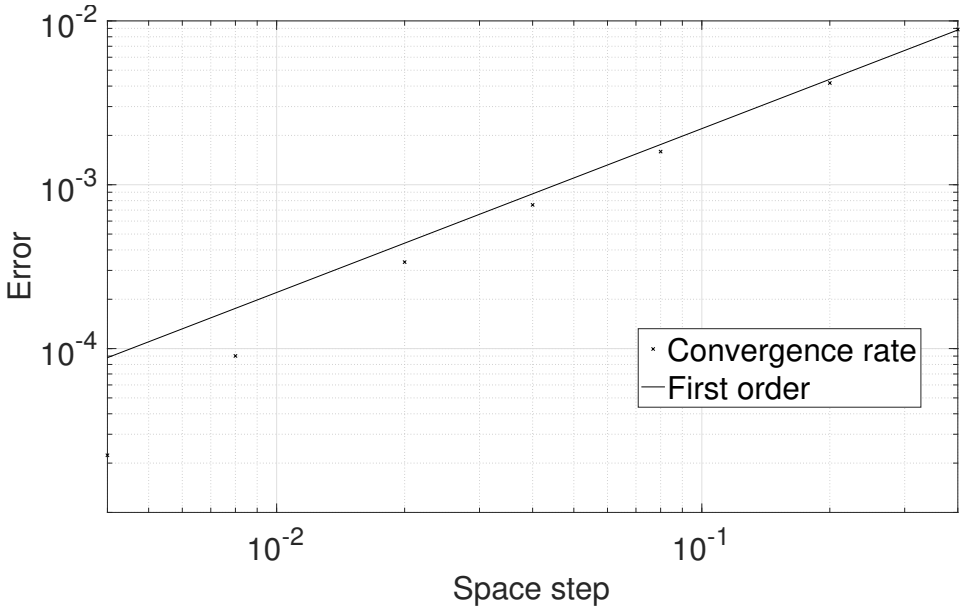

FIGURE 3. Return to equilibrium: L^2-convergence rate for δ_G compared to first order

Remark 1. *Note that in a symmetric case, the two first equalities in* (29) *become* $F_\chi = T_\theta = 0$. *In fact, in this particular case,* $\int_{\Omega_x} p_\eta \partial_x \mathcal{R}\,\mathrm{d}x = 0$ *and* $\int_{\Omega_x} p_\eta \partial_\theta \mathcal{R}\,\mathrm{d}x = 0$. *Although neither horizontal nor angular acceleration should be noticed in such a*

ω	0.1	0.25	0.5	0.75	0.9
$\overline{\delta_t}$	6.21×10^{-4}	7.69×10^{-4}	1.25×10^{-3}	1.47×10^{-3}	1.61×10^{-3}
$\#_{resol}$	26	35	46	82	192

TABLE 3.A. Throwing: The mean time step, the mean number of calls of the linear system resolution for different values of ω.

configuration, see (5)*, in practice, due to the fixed point error, small oscillations can appear in long time. For this reason, even with an axisymmetric buoy* (29) *is imposed.*

4.2. **Throwing.** To show the robustness of the code, a simulation of a buoy falling into the water and floating freely is shown.

In a closed domain of length $l = 4$ with a flat bottom, a buoy is thrown on the water at rest, i.e. $\phi^0 = g$ and $u^0 = 0$ with $F_\chi = 0$, $F_\zeta = 0$ and $T_\theta = 0$. The buoy is an ovoid parametrized by $(0.3\cos(s) + 0.025\cos(2s), 0.2\sin(s))$ for $s \in [0, 2\pi]$. The initial value of the buoy velocity is $\dot{\chi}^0 = 1.0$, $\dot{\zeta}^0 = 1.0$ and $\dot{\theta}^0 = 1.0$. The initial position of the ovoid is defined by $\chi^0 = 0.4$, $\zeta^0 = 1.5$ and $\theta^0 = \dfrac{\pi}{2}$. The mass and the angular moment of the buoy are taken equal to 5×10^{-3} and 1×10^{-3}.

Taking 1000 grid points, the space step is $\delta_x = 4.0 \times 10^{-3}$ and the final time $\mathcal{T}$ is equal to 1.5.

The buoy position, the water height and the surface pressure at different times are shown in Figure 4. At the beginning the fluid is at rest and the buoy is not in contact with the fluid. At the impact an energy transfer from the buoy to the water is observed and small waves are created. The buoy continues moving to the right and moreover angular and vertical oscillations are observed. The evolution of the mechanical energy in time is shown in Figure 5. More precisely the energy ratio $\dfrac{\sum_{k\in\mathbb{T}} \delta_x \mathcal{E}_k(t) + E(t)}{\sum_{k\in\mathbb{T}} \delta_x \mathcal{E}_k(0) + E(0)}$ is shown. The result is in accordance with Proposition 3. More precisely a dissipation of the mechanical energy is observed. The fixed point converges with a mean time step of 7.69×10^{-4} and the mean number of calls of the linear system resolution per time step is equal to 35. This seems satisfactory in terms of numerical costs. The mean time step $\overline{\delta_t}$ (second row) and the mean number of calls $\#_{resol}$ of the linear system resolution per time step (third row) for different values of the time step reduction factor ω (first row) are shown in Table 3.a.

By increasing the parameter ω, the mean time step as well as the mean linear system resolutions per time step increase. This seems natural but makes the choice for an optimal value quite difficult. More precisely the CPU time decreases with a bigger time step but increases with the number of calls of the linear system resolution. As a consequence the choice for ω highly depends on the test case.

4.3. **Wave energy converter.** To simulate an energy converter, a spring is added to the modelization from section 2.2, see Figure 6. A restoring as well as damping force will be taken into account to modelize the energy extraction. The structure is allowed to move vertically, rotate around its center of mass and is fixed in the horizontal direction, i.e. $F_\zeta = -c\dot{\zeta} - K\left(\zeta - \overline{\zeta}\right)$, $T_\theta = 0$ and $F_\chi = \int_{\Omega_x} p_\eta \partial_x \mathcal{R}\, \mathrm{d}x$. The damping (resp. stiffness) coefficients are denoted $c \in \mathbb{R}_+$ (resp. $K \in \mathbb{R}_+$). The

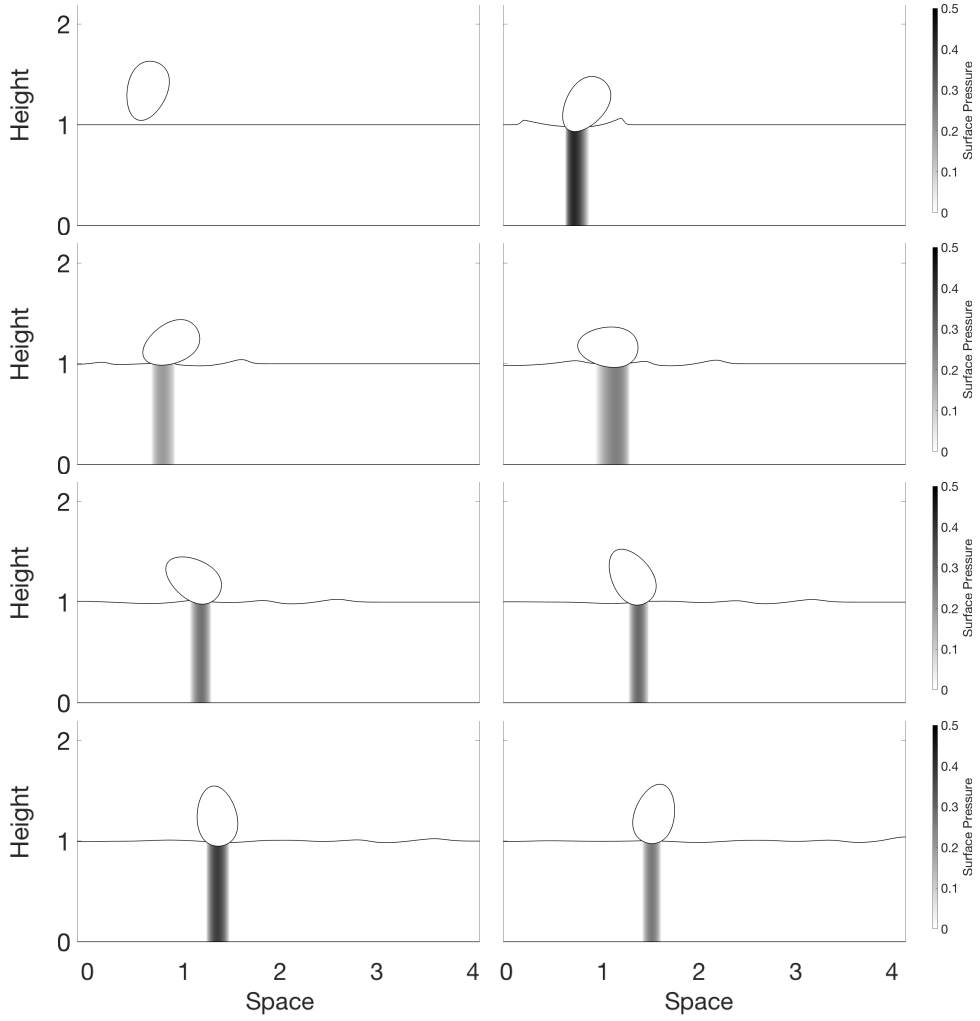

FIGURE 4. Throwing: buoy, water height and surface pressure from $t = 0.3$ to $t = 1.35$ at regular intervals

characteristic length of the spring is denoted $\overline{\zeta}$. Let us rewrite the equations from section 2.2 where we add a spring. The proofs will not be detailed since they are an adaptation of the equivalent results cited previously.

The planar movement of the energy wave converter is described by the system

$$\left\{ \begin{array}{l} M\ddot{\zeta} = -Mg + \displaystyle\int_{\Omega_x} p_\eta \mathrm{d}x - c\dot{\zeta} - K\left(\zeta - \overline{\zeta}\right) \\ \mathcal{J}_G\ddot{\theta} = \displaystyle\int_{\Omega_x} p_\eta \partial_\theta \mathcal{R} \mathrm{d}x. \end{array} \right. \tag{32}$$

The energy for the solid can be written.

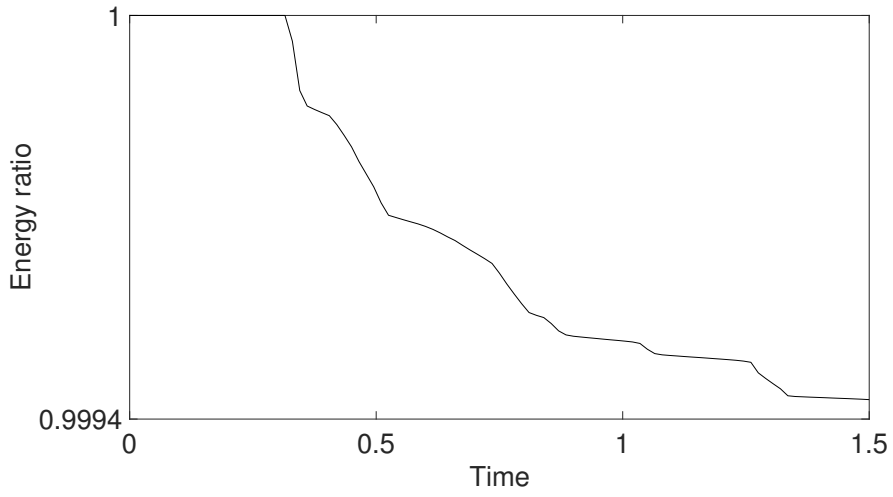

FIGURE 5. Throwing: mechanical energy ratio evolution in time

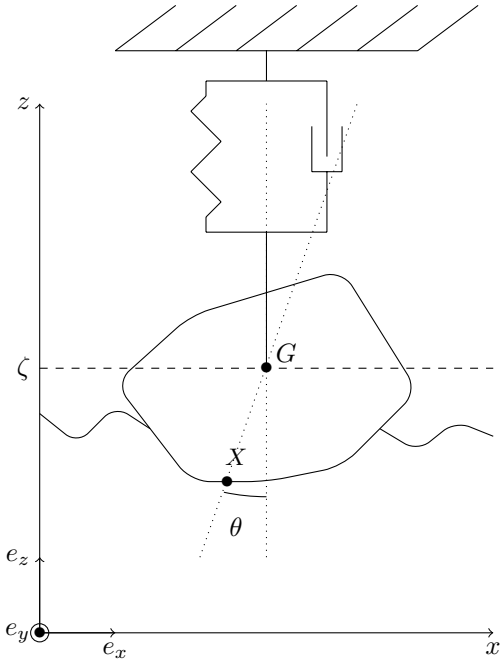

FIGURE 6. Wave energy converter with a spring

Lemma 4.1. *Any smooth solution of* (32) *satisfies the following energy law*

$$\partial_t \widetilde{E} = \int_{\Omega_x} p_\eta \partial_\theta \mathcal{R}\, \mathrm{d}x\dot{\theta} + \int_{\Omega_x} p_\eta\, \mathrm{d}x\dot{\zeta} - c\dot{\zeta}^2$$

with $\widetilde{E}(\zeta,\theta) = \dfrac{\mathcal{J}_G}{2}\dot{\theta}^2 + \dfrac{M}{2}\dot{\zeta}^2 + Mg\zeta + \dfrac{K}{2}\left(\zeta - \overline{\zeta}\right)^2$.

The energy for the coupled fluid-solid system is obtained.

Proposition 4. *Considering a no-flux boundary on Ω_x, any smooth solution of (32) and (1)-(2) satisfies the following energy balance law*

$$\partial_t \left(\int_{\Omega_x} \mathcal{E} \, \mathrm{d}x + \widetilde{E} \right) = \int_{\Omega_x} (p_\eta + gh) \, \partial_t B \mathrm{d}x - c\dot{\zeta}^2.$$

The term $c\dot{\zeta}^2$ is a dissipation term due to the damping of the spring. A part of this energy could be recovered for energy production.

Using again the Newmark scheme (16) with $\widetilde{\Lambda} = \begin{pmatrix} \zeta \\ \theta \end{pmatrix}$, (32) is discretized in the following way

$$\text{(33)} \qquad \begin{cases} M\ddot{\zeta}^n = -Mg + \displaystyle\sum_{k\in\mathbb{T}} |k| p_k^n - c\dot{\zeta}^n - K\left(\zeta^n - \overline{\zeta}\right) \\ \mathcal{J}_G \ddot{\theta}^n = \displaystyle\sum_{k\in\mathbb{T}} |k| p_k^n \partial_\theta^\delta R_k^n. \end{cases}$$

As before the discrete energy stability is proven for the adapted discretization of $\partial_\theta^\delta R_k^n$. Let us first recall the energy for the Newmark scheme.

Lemma 4.2. *Let $\alpha = \beta = 1$. Then the scheme (16) and (33) satisfies the following energy law*

$$\begin{aligned} \partial_t^{n+1} \left(\widetilde{E} + \frac{\delta_t^{n+1}}{4} \left(\dot{\zeta}\right)^2 \right) \quad = \quad & \sum_{k\in\mathbb{T}} \left(|k| p_k^{n+1} \partial_\theta^\delta R_k^{n+1} \right) \partial_t^{n+1} \theta + \sum_{k\in\mathbb{T}} |k| p_k^n \partial_t^{n+1} \zeta \\ & - P_c^{n+1} - K \frac{\delta_t^{n+1}}{2} \left(\partial_t^{n+1} \zeta\right)^2 \end{aligned}$$

with $\widetilde{E}^n = \widetilde{E}\left(\zeta^n, \theta^n\right)$ and $P_c^{n+1} = \dfrac{c}{2} \left(\partial_t^{n+1} \zeta\right)^2 + \dfrac{c}{2} \left(\dfrac{\dot{\zeta}^{n+1} + \dot{\zeta}^n}{2} \right)^2$.

Proof. The proof is similar to the proof of Lemma 3.2. The coefficients are (with obvious notations) $\widetilde{f}^n = \begin{pmatrix} -Mg + K\overline{\zeta} + \displaystyle\sum_{k\in\mathbb{T}} |k| p_k^n \\ \displaystyle\sum_{k\in\mathbb{T}} |k| p_k^n \partial_\theta^\delta R_k^n \end{pmatrix}$, $\widetilde{C}_1 = \begin{pmatrix} M & 0 \\ 0 & \mathcal{J}_G \end{pmatrix}$, $\widetilde{C}_2 = \begin{pmatrix} c & 0 \\ 0 & 0 \end{pmatrix}$ and $\widetilde{C}_3 = \begin{pmatrix} K & 0 \\ 0 & 0 \end{pmatrix}$. □

For the adapted choice of discretization for $\partial_\theta^\delta R_k^n$, see (25), the energy stability is achieved for the coupled fluid-solid system. Note that $\partial_t^n \chi = 0$ in (25) since the structure is fixed in the horizontal direction.

Proposition 5. *Consider a no-flux boundary on Ω_x and let $\alpha = \beta = 1$, then the scheme (11)-(13), (16) and (33) with (25) admits the following dissipation law*

$$\begin{aligned} \partial_t^{n+1} \left(\sum_{k\in\mathbb{T}} |k| \mathcal{E}_k + \widetilde{E} + \frac{\delta_t^{n+1}}{4} \left(\dot{\zeta}\right)^2 \right) \leq \quad & \sum_{k\in\mathbb{T}} \left(|k| \left(g h_k^n + p_k^{n+1} \right) \partial_t^{n+1} B_k \right) \\ & - P_c^{n+1} - K \frac{\delta_t^{n+1}}{2} \left(\partial_t^{n+1} \zeta\right)^2. \end{aligned}$$

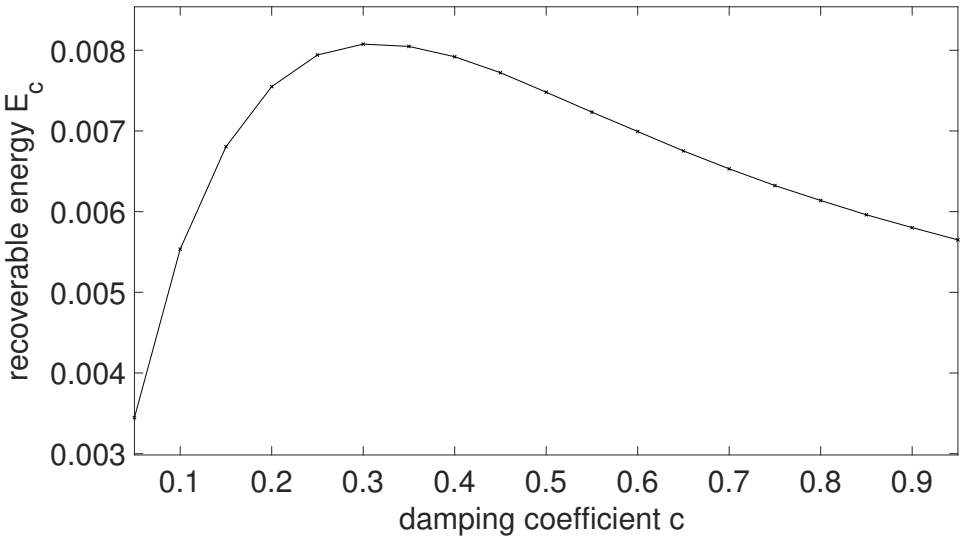

FIGURE 7. Spring: recoverable energy for different values of the damping coefficient

In the following a simple case of a wave energy converter attached to a spring is simulated.
The buoy is an ellipse with semi-minor and semi-major axis respectively equal to 0.2 and 0.4. Its mass is equal to 1.0×10^{-2} and the moment of inertia around G equals 5.0×10^{-3}. The stiffness coefficients K and the characteristic length $\overline{\zeta}$ are 1.0×10^{-2} respectively 1.4. At the left boundary waves of the form $h\,(t) = h^0 + 0.05 \sin\,(4\pi t)$ enter the domain. At the right boundary we impose a non-flux boundary condition. Furthermore the initial horizontal and vertical coordinates of the center of mass are 1.5 respectively 1.4. Initially $\dot{\zeta} = 0$, $\theta^0 = \frac{\pi}{2}$, $\dot{\theta}^0 = 0$, $\overline{u}^0 = 0$ and $\phi^0 = \phi_0$ so that the buoy is at equilibrium, see Section 4.1

Taking 1000 grid points and a domain with flat bottom of length $l = 3$, the space step $\delta_x = 3.0 \times 10^{-3}$. The final time $\mathcal{T}$ is equal to 1.

The optimisation of wave energy converters is a key point in the development of such machines. To show the feasibility of an optimisation procedure, a naive estimation of the recoverable energy is done. The recovered energy, depending on the technology used to convert wave energy, is a part of the recoverable energy defined by

$$E_c = \sum_{n \in \{1,\dots,N\}} \delta_t^n P_c^n$$

where N is the number of time iterations and P_c^n defined in Lemma 4.2. In Figure 7 the recoverable energy is shown for different values of c.

The best choice seems to be obtained for $c = 0.3$. Physically a small stiffness allows the spring to move as much as possible. Furthermore a small damping coefficient would not be able to absorb any energy. In contrary if the damping coefficient is too high, the buoy will be slowed down due to the damping and the recoverable energy would not be optimal.

5. Conclusion

A strong coupling between a congested shallow water type model and Newton's second law of motion is presented for the modeling of floating structures. We have taken a particular care to the energy transfer between the solid and the water. An entropy correction is made at the discrete level in order to ensure an entropy dissipation law and the numerical scheme proposed in [12] is adapted to take into account a freely floating object. Finally numerical simulations are proposed to validate the approach and to show the feasibility of physically relevant cases.

However real life applications need an extension to the two dimensional case. A first step towards real life applications, i.e. the coupling was analyzed in this paper. Since the computations become CPU costly in higher dimensions, some scientific computing issues should be resolved beforehand. One can think of linking our method with a less CPU consuming scheme for free surface flow far from the congested area.

The physical description of water waves is important when considering wave energy converters. More complex models such as dispersive models [7, 21] or layerwise models [2] or the combination of both [11] could be used to represent the flow. Dispersive models do not neglect the vertical acceleration and are therefore more adapted to characterize heave effets. Layerwise models can better modelize wind effects by considering a vertical profile of the velocity. Since our approach only concerns the water height and not the velocity, the numerical resolution of the cited models should not raise particular difficulties.

A logical follow-up is the interaction of several objects for the simulation of wave energy converter farms [27] or floating fragments during inondations. Since these phenomena take place on a large space scale, the proposed model seems well adapted. Our method is directly adaptable to take into account several objets. Nevertheless for the latter, interactions between the objets should be accounted for.

A challenging objective is the handling of submerged objets [10, 13]. This issue seems related to layerwise models since at least two water heights are necessary. However the transition between a totally submerged and a floating objet is still open at the moment. Some energy converters also interact with the bottom [3, 4].

Acknowledgments

The authors wish to express their warm thanks to Cindy Guichard for many fruitful discussions and kind advices. This research is part of a collaborative program with the ANR-FEM (France Energies Marines) project HYFLOEFLU through the project call ITE EMR 2015.

References

[1] Agamloh, E., Wallace, A., and von Jouanne, A. Application of fluid-structure interaction simulation of an ocean wave energy extraction device. *Renewable Energy 33*, 4 (2008), 748–757.

[2] Audusse, E., Bristeau, M.-O., Perthame, B., and Sainte-Marie, J. A multilayer Saint-Venant system with mass exchanges for shallow water flows. Derivation and numerical validation. *ESAIM: Mathematical Modelling and Numerical Analysis 45*, 1 (2011), 169–200.

[3] Benyo, K. Wave-structure interaction for long wave models with a freely moving bottom. working paper or preprint <hal-01665775>, 2017.

[4] Benyo, K. Numerical analysis of the weakly nonlinear Boussinesq system with a freely moving body on the bottom. working paper or preprint <arXiv-1805.07216 >, 2018.

[5] Bocchi, E. Floating structures in shallow water: local well-posedness in the axisymmetric case. working paper or preprint <arXiv-1802.07643>, 2018.
[6] Bosi, U., Engsig-Karup, A. P., Eskilsson, C., and Ricchiuto, M. A spectral/hp element depth-integrated model for nonlinear wave-body interaction. Research Report RR-9166, Inria Bordeaux Sud-Ouest ; Technical University of Denmark ; University of Aalborg ; RISE, 2018.
[7] Bristeau, M.-O., Mangeney, A., Sainte-Marie, J., and Seguin, N. An energy-consistent depth-averaged Euler system: derivation and properties. *Discrete and Continuous Dynamical Systems - Series B 20*, 4 (2015), 961–988.
[8] Cancès, C., and Guichard, C. Numerical analysis of a robust free energy diminishing finite volume scheme for parabolic equations with gradient structure. *Foundations of Computational Mathematics 17*, 6 (2017), 1525–1584.
[9] Chabannes, V. *Vers la simulation numérique des écoulements sanguins*. Thèse, Université de Grenoble, 2013.
[10] Ducassou, B., Nuñez, J., Cruchaga, M., and Abadie, S. A fictitious domain approach based on a viscosity penalty method to simulate wave/structure interaction. *Journal of Hydraulic Research 55*, 6 (2017), 847–862.
[11] Fernandez-Nieto, E. D., Parisot, M., Penel, Y., and Sainte-Marie, J. A hierarchy of non-hydrostatic layer-averaged approximation of Euler equations for free surface flows. working paper or preprint <hal-01324012>, 2017.
[12] Godlewski, E., Parisot, M., Sainte-Marie, J., and Wahl, F. Congested shallow water model: roof modelling in free surface flow. *ESAIM: Mathematical Modelling and Numerical Analysis* (2018).
[13] Guerber, E. *Numerical modelling of nonlinear interactions of waves with submerged structures : applied to the simulation of wave energy converters*. Thèse, Université Paris-Est, 2011.
[14] Harris, J., Kuznetsov, K., Peyrard, C., Saviot, S., Mivehchi, A., T. Grilli, S., and Benoit, M. Simulation of wave forces on a gravity based foundation by a BEM based on fully nonlinear potential flow. In *27th Offshore and Polar Engineering Conference* (San Francsico, USA, 2017).
[15] Iguchi, T., and Lannes, D. Hyperbolic free boundary problems and applications to wave-structure interactions. working paper or preprint <arXiv-1806.07704>, 2018.
[16] John, F. On the motion of floating bodies. I. *Communications on Pure and Applied Mathematics 2*, 1 (1949), 13–57.
[17] Kashiwagi, M. Non-linear simulations of wave-induced motions of a floating body by means of the mixed Eulerian-Lagrangian method. *Proceedings of the Institution of Mechanical Engineers, Part C: Journal of Mechanical Engineering Science 214*, 6 (2000), 841–855.
[18] Knudsen, J., and Hjorth, P. *Elements of Newtonian Mechanics*. Springer Berlin Heidelberg, 2012.
[19] Krenk, S. Energy conservation in Newmark based time integration algorithms. *Computer methods in applied mechanics and engineering 195*, 44 (2006), 6110–6124.
[20] Lannes, D. On the dynamics of floating structures. *Annals of PDE 3*, 1 (2017), 11.
[21] Lannes, D., and Bonneton, P. Derivation of asymptotic two-dimensional time-dependent equations for surface water wave propagation. *Physics of Fluids 21*, 1 (2009), 016601.
[22] LeVeque, R. J. *Finite volume methods for hyperbolic problems*. Cambridge University Press, 2002.
[23] Matt, F., Babarit, A., Ben, C., David, F., Louise, O., Katie, S., Johannes, S., and Troch, P. A review of numerical modelling of wave energy converter arrays. In *ASME 2012 International Conference on Ocean, Offshore and Artic Engineering* (Rio de Janeiro, Brazil, 2012).
[24] Palm, J., Eskilsson, C., Moura Paredes, G., and Bergdahl, L. CFD simulation of a moored floating wave energy converter. In *Proceedings of the 10th European Wave and Tidal Energy Conference* (Aalborg, Denmark, 2013).
[25] Parisot, M., and Vila, J.-P. Centered-Potential Regularization for the advection upstream splitting method. *SIAM Journal on Numerical Analysis 54*, 5 (2016), 3083–3104.
[26] Parolini, N., and Quarteroni, A. Mathematical models and numerical simulations for the America's cup. *Computer Methods in Applied Mechanics and Engineering 194*, 9 (2005), 1001–1026.

[27] Penalba, M., Touzón, I., Lopez-Mendia, J., and Nava, V. A numerical study on the hydrodynamic impact of device slenderness and array size in wave energy farms in realistic wave climates. *Ocean Engineering 142* (2017), 224–232.
[28] Quarteroni, A., Tuveri, M., and Veneziani, A. Computational vascular fluid dynamics: problems, models and methods. *Computing and Visualization in Science 2*, 4 (2000), 163–197.
[29] Wu, G., and Taylor, R. The coupled finite element and boundary element analysis of nonlinear interactions between waves and bodies. *Ocean Engineering 30*, 3 (2003), 387–400.
[30] Yu, Y.-H., and Li, Y. Reynolds-averaged Navier–Stokes simulation of the heave performance of a two-body floating-point absorber wave energy system. *Computers & Fluids 73* (2013), 104–114.

E-mail address: edwige.godlewski@upmc.fr
E-mail address: martin.parisot@inria.fr
E-mail address: jacques.sainte-marie@inria.fr
E-mail address: fabien.wahl@upmc.fr

Sorbonne Université, université Paris-Diderot SPC, Cerema, CNRS, Inria, laboratoire Jacques-Louis Lions, LJLL, ANGE team, F-75005 Paris, France